

Beyond Single-Shot Fidelity: Chernoff-Based Throughput Optimization in Superconducting Qubit Readout

Sinan Bugu^{1,2,*}

¹*Department of Physics and Astronomy, North Carolina State University, Raleigh, North Carolina, USA*

²*BuQuLab Research Laboratory, Winston-Salem, North Carolina, USA*

(Dated: March 5, 2026)

Single-shot fidelity is the standard benchmark for superconducting qubit readout, yet it does not directly minimize the wall-clock time needed to certify a quantum state. We treat the dispersive measurement record as a stochastic communication channel and compute the classical Chernoff information governing the multi-shot error exponent, using a trajectory model that incorporates T_1 relaxation with full cavity memory. The integration time that maximizes single-shot fidelity and the time that minimizes total certification time do not coincide. For representative transmon parameters and hardware overheads, the throughput-optimal window is longer, cutting certification time by roughly 9–11%, with the gain saturating near $1.13\times$ in the high-readout-power and high-overhead regime. Benchmarking the extracted classical information against the unit-efficiency Gaussian Chernoff limit defines an information-extraction efficiency: dispersive schemes capture $\sim 45\%$ at short integration times, dropping to $\eta_{\text{info}}(\tau_{\text{rate}}) \approx 12\%$ at $\tau_{\text{rate}} \approx 1.22 \mu\text{s}$ as T_1 -induced trajectory smearing accumulates. These results connect readout calibration directly to the operational objective of minimizing certification time in high-throughput superconducting processors.

Keywords: Superconducting qubits, Dispersive readout, Chernoff error exponent, Quantum hypothesis testing, Readout calibration, Throughput optimization, Transmon

I. INTRODUCTION

The scaling of superconducting quantum processors toward the fault-tolerant regime demands not only high-fidelity operations but also fast certification cycles [1, 2]. Recent surface-code demonstrations have identified cycle time as a critical bottleneck [3, 4], with system-level latencies in large-scale processors often dominating total execution time [5]. Within the circuit quantum electrodynamics (cQED) architecture, dispersive readout of transmon qubits remains one of the most persistent performance constraints [6, 7], despite advances in dynamic control of the dispersive interaction [8]. Coherent gates now operate on nanosecond timescales, yet measurement windows remain disproportionately long relative to intrinsic device dynamics [9, 10].

This latency reflects a trade-off inherent to dispersive measurement. Stronger drives accelerate information extraction but also enhance measurement-induced dephasing, AC Stark shifts, and transitions into non-computational leakage manifolds [11–14]. At sufficiently high powers these effects escalate into transmon ionization [15] and stochastic state transitions arising from breakdown of the dispersive approximation [16]. Alternative coupling architectures have been explored to enable faster measurement while reducing backaction, including longitudinal interaction schemes [17] and the quarton coupler enabling nanosecond-scale readout windows [18]. Integrated filtering and Purcell-protected designs further suppress measurement-induced decay in high-power regimes [19].

Standard readout practice optimizes by maximizing single-shot Bayes fidelity [20]. Model-based approaches have extended this to systematic suppression of assignment and leakage errors in multi-qubit architectures [21]. For protocols involving repeated measurements, however, single-shot fidelity does not capture the cumulative cost of leakage and hardware latency [22]. Multiplexed readout [23, 24], active reset [25], and near-quantum-limited amplification [26, 27] have all improved raw measurement performance, but scalable architectures ultimately need to minimize the wall-clock time to reach a target confidence level ϵ . As argued in the context of decentralized certification [28, 29], this shifts optimization from isolated decision accuracy toward certification throughput — and with it, the fidelity-optimal integration time τ_{fid} may be suboptimal once hardware latency and reset constraints enter [30].

We evaluate readout through an information-theoretic lens, treating measurement score distributions as probability objects rather than isolated binary outcomes [29, 31]. The role of Chernoff information as a figure of merit for qubit readout has been established [32], with asymptotic optimality grounded in hypothesis testing theory [33, 34]. Prior work has primarily addressed repetitive measurement statistics in platform-agnostic settings; here we apply this framework to continuous-time dispersive transmon readout with stochastic T_1 relaxation and explicit hardware latency.

Our central contribution is to frame readout calibration as a wall-clock certification problem. Rather than maximizing single-shot fidelity, we minimize the total certification time

$$T_{\text{cert}}(\tau) = \frac{\log(1/\epsilon)}{C(\tau)}(\tau + \tau_{\text{oh}}), \quad (1)$$

* sbugu@ncsu.edu; sinanbugu@gmail.com

which incorporates both the classical Chernoff information $C(\tau)$ and the fixed per-shot overhead τ_{oh} . Score distributions are modeled with Gaussian noise kernels, subsequently deformed by T_1 relaxation events that produce asymmetric tails and assignment errors [10], consistent with experimental observations [7, 20]. Using a trajectory model with full cavity memory [35], we show that τ_{fid} and the throughput-optimal time τ_{rate} are generically distinct — a separation that persists even in the long-coherence limit.

Beyond numerical optimization, we derive asymptotic scaling laws showing that any nonzero hardware overhead shifts the throughput optimum toward longer integration times. We further introduce an experimentally accessible diagnostic by benchmarking classical Chernoff capture against the unit-efficiency Gaussian Chernoff limit [36, 37]. Together, these results provide a calibration procedure for high-duty-cycle superconducting processors, where the interplay between speed, noise, and nonlinearity in dispersive measurement [38, 39] makes careful optimization of temporal resources necessary.

II. STOCHASTIC COMMUNICATION MODEL OF DISPERSIVE READOUT

A. Dispersive Dynamics and Homodyne SNR

We model dispersive readout of a transmon qubit coupled to a readout resonator, described by the Hamiltonian $H/\hbar = \omega_r a^\dagger a + \frac{\omega_q}{2} \sigma_z + \chi a^\dagger a \sigma_z$ [40]. Under a constant microwave drive, the displacement of the cavity coherent states $|\pm \alpha(t)\rangle$ depends on the qubit state. The separation between these states along the measured quadrature grows according to the cavity response function:

$$\Delta\alpha(t) = \frac{4\chi}{\kappa} \left(1 - e^{-\kappa t/2}\right) \quad (2)$$

where χ is the dispersive shift and κ is the cavity linewidth [10].

The information reaching the homodyne detector is processed via a matched filter to maximize the signal-to-noise ratio (SNR) [9, 35]. The filter weighting $h(t) = \Delta\alpha(t)$ is chosen to match the expected signal shape. For a given integration time τ , the squared signal-to-noise ratio at the detector is:

$$\text{SNR}^2(\tau) = \eta \kappa \bar{n} \int_0^\tau |\Delta\alpha(t)|^2 dt \quad (3)$$

where η is the overall quantum efficiency and \bar{n} is the steady-state photon number. We define the matched-filter score as a normalized projection variable whose conditional noise variance is unity. In this convention, detector inefficiency η enters exclusively through the mean separation encoded in $\text{SNR}(\tau)$, while the additive noise variance of the score distribution is fixed to one. The statistical structure of these distributions determines the

persistence of quantum signatures under noise [41, 42]. While we assume a standard homodyne detection chain, on-chip microwave photon counters have demonstrated comparable performance by mapping quantum information directly into binary click statistics [43].

B. Stochastic Trajectory Smearing with Cavity Memory

To accurately represent the excited state distribution $p_e(x)$, we account for stochastic relaxation of the qubit from $|e\rangle$ to $|g\rangle$ at a jump time $t_j \in [0, \tau]$. We adopt a trajectory model that enforces continuity of the cavity field at the jump time. For $t < t_j$, the system follows the excited-state trajectory $\alpha(t) = +\Delta\alpha(t)$. At the moment of the jump, the cavity field is at $+\Delta\alpha(t_j)$. For $t > t_j$, it relaxes exponentially toward the ground-state trajectory $-\Delta\alpha(t)$ at rate $\kappa/2$:

$$\alpha(t > t_j) = -\Delta\alpha(t) + 2\Delta\alpha(t_j)e^{-\kappa(t-t_j)/2} \quad (4)$$

This expression enforces continuity at the jump boundary, $\alpha(t_j^-) = \alpha(t_j^+) = \Delta\alpha(t_j)$. The readout drive remains on throughout the integration window, so after a decay event the cavity relaxes toward the driven ground-state trajectory rather than the undriven vacuum. The matched-filter score $s(t_j)$ is calculated by projecting this continuous trajectory onto the filter $h(t)$. The full excited state distribution is then:

$$p_e(x) = e^{-\tau/T_1} \mathcal{N}(\mu_e, 1) + \int_0^\tau \frac{1}{T_1} e^{-t_j/T_1} \mathcal{N}(\mu(t_j), 1) dt_j \quad (5)$$

where the first term accounts for trajectories where no decay occurs during the integration window.

C. Certification Wall-Clock Time Objective

We formulate certification as a binary hypothesis test between $p_g(x)$ and $p_e(x)$, following the information-theoretic perspective of [28, 29]. Distinguishability is quantified via the classical Chernoff information [33, 44]:

$$C = -\log \left(\min_{s \in [0, 1]} \int p_g(x)^s p_e(x)^{1-s} dx \right) \quad (6)$$

The objective is to minimize the total wall-clock time required to certify the qubit state to a target error probability ϵ . With per-shot hardware overhead τ_{oh} accounting for control latency, resonator depletion, and reset timing [3, 4], the certification time is:

$$T_{\text{cert}}(\tau) = \frac{\log(1/\epsilon)}{C(\tau)} (\tau + \tau_{\text{oh}}) \quad (7)$$

The Chernoff information characterizes the asymptotic large-shot error exponent. For the target error levels

considered here the required number of repetitions can be modest; we therefore use $C(\tau)$ as a throughput proxy and focus on the location of the certification-time minimum rather than finite-sample corrections to the exponent.

We numerically minimize $T_{\text{cert}}(\tau)$ to find the throughput-optimal integration time τ_{rate} , and compare it to the fidelity-optimal time τ_{fid} , obtained by maximizing $F = 1 - \frac{1}{2} \int \min(p_g, p_e) dx$. The speedup factor is:

$$\text{Speedup} = \frac{T_{\text{cert}}(\tau_{\text{fid}})}{T_{\text{cert}}(\tau_{\text{rate}})} \quad (8)$$

We isolate the physical degradation of the measurement channel by defining a unit-efficiency Gaussian Chernoff benchmark

$$C_{\text{ideal}}(\tau) = \frac{1}{8} \kappa \bar{n} \int_0^\tau |\Delta\alpha(t)|^2 dt, \quad (9)$$

corresponding to the classical Chernoff information with $T_1 \rightarrow \infty$ and $\eta = 1$. This provides a baseline against which we quantify information loss from detector inefficiency and T_1 -induced trajectory smearing. All reported curves are obtained from deterministic numerical integration of the score distributions without stochastic sampling. Convergence with respect to discretization of the score grid, time grid, and decay-time quadrature was verified; residual numerical errors are smaller than the marker size in all figures.

D. Asymptotic Scaling and Overhead-Induced Shift

To understand the structural origin of the separation between τ_{fid} and τ_{rate} , we consider the long-coherence limit ($T_1 \rightarrow \infty$) where score distributions remain symmetric Gaussians. In this regime the classical Chernoff information reduces to

$$C(\tau) = \frac{\text{SNR}^2(\tau)}{8}. \quad (10)$$

The throughput objective (7) is then equivalent, up to a constant prefactor, to minimizing

$$T_{\text{cert}}(\tau) \propto \frac{\tau + \tau_{\text{oh}}}{\text{SNR}^2(\tau)}. \quad (11)$$

A stationary point satisfies

$$\begin{aligned} \frac{d}{d\tau} \left(\frac{\tau + \tau_{\text{oh}}}{\text{SNR}^2(\tau)} \right) &= 0 \\ \iff \text{SNR}^2(\tau) &= (\tau + \tau_{\text{oh}}) \frac{d}{d\tau} \text{SNR}^2(\tau). \end{aligned} \quad (12)$$

For dispersive readout with finite resonator linewidth, $\text{SNR}^2(\tau)$ is not perfectly linear in τ because of cavity ring-up. Using $\Delta\alpha(t) \propto (1 - e^{-\kappa t/2})$, the integrand entering $\text{SNR}^2(\tau) \propto \int_0^\tau \Delta\alpha(t)^2 dt$ contains both $e^{-\kappa t/2}$ and $e^{-\kappa t}$ terms, giving initially sublinear growth that crosses

over to an asymptotically linear regime. This early-time curvature regularizes the optimization and yields a well-defined interior minimum of $T_{\text{cert}}(\tau)$.

It is instructive to contrast this with a purely linear surrogate $\text{SNR}^2(\tau) \approx a\tau + b$ valid only deep in the steady-state regime. Substituting gives

$$T_{\text{cert}}(\tau) \propto \frac{\tau + \tau_{\text{oh}}}{a\tau + b}, \quad \frac{dT_{\text{cert}}}{d\tau} \propto \frac{b - a\tau_{\text{oh}}}{(a\tau + b)^2}, \quad (13)$$

which is monotonic in τ and cannot produce an interior optimum. The existence and location of τ_{rate} therefore depend on the finite ring-up dynamics captured by the full cavity-memory model.

Equation (12) makes the overhead-induced shift transparent. Increasing τ_{oh} raises the right-hand side, pushing τ_{rate} toward larger integration times: when fixed temporal costs are nonzero, extracting more information per shot becomes advantageous. The rightward shift of the throughput optimum is therefore not a decoherence artifact but a structural consequence of optimizing wall-clock certification time, present even at $T_1 \rightarrow \infty$. In practice, the crossover between ring-up and linear regimes of $\text{SNR}^2(\tau)$ can produce two competing local minima at very small overheads; for the physically relevant range $\tau_{\text{oh}} \gtrsim 5 \mu\text{s}$ the global minimum is unique and shifts monotonically with overhead.

III. RESULTS

We evaluate the optimization framework using parameters representative of contemporary superconducting circuit architectures: dispersive shift $\chi/2\pi = 1.2$ MHz, cavity linewidth $\kappa/2\pi = 5.0$ MHz, and steady-state photon number $\bar{n} = 80$. Unless otherwise stated, we take detection efficiency $\eta = 0.45$ and qubit relaxation time $T_1 = 30 \mu\text{s}$. Dispersive shifts in the MHz range and cavity linewidths of several MHz are routinely reported in high-fidelity readout experiments [7, 20]. Average photon numbers $\bar{n} \sim 50$ –100 and measurement efficiencies $\eta \approx 0.4$ –0.6 are consistent with modern high-efficiency readout implementations [11, 45], while relaxation times $T_1 \sim 20$ –50 μs are typical of contemporary transmon platforms [46].

The per-shot overhead $\tau_{\text{oh}} = 15 \mu\text{s}$ is treated as a lumped system-level latency parameter incorporating classical control processing, resonator depletion, and reset timing constraints. Experimental studies of active resonator reset and measurement-feedback cycles show that cavity depletion and control-flow latency can occupy a substantial fraction of the measurement cycle, particularly in architectures prioritizing Purcell protection and coherence [30, 47]. Optimized fast-reset protocols can reduce this overhead, but realistic superconducting control stacks commonly retain microsecond-scale latencies, motivating the explicit τ_{oh} term in the throughput analysis.

A. Information Accumulation and Trajectory Smearing

Information accumulation is governed by the cavity response and the subsequent smearing of score distributions from qubit decay. Figure 1(a) shows the growth of cavity state separation $\Delta\alpha(t)$, which approaches its steady-state value on a timescale set by κ^{-1} . The integrated information, quantified by $SNR^2(\tau)$, grows nonlinearly during ring-up before entering a linear regime [Fig. 1(b)]. At $\tau = 1.0 \mu\text{s}$, the score distributions $p_g(x)$ and $p_e(x)$ are clearly separated, though $p_e(x)$ exhibits a tail extending toward the ground-state mean due to T_1 events [Fig. 1(c)].

T_1 -induced smearing introduces asymmetry between the two hypotheses. Figure 2(a) compares the excited state distribution with and without relaxation; decay events shift the optimal Chernoff parameter s^* away from the symmetric Gaussian value of 0.5 [Fig. 2(b)]. As τ increases, s^* drops sharply — the optimal classifier becomes increasingly biased against assigning the excited state to scores that could have resulted from a decay event.

The information extraction efficiency η_{info} is defined as the ratio of classical Chernoff information $C(\tau)$ to the unit-efficiency Gaussian benchmark $C_{\text{ideal}}(\tau)$. As shown in Fig. 2(c), η_{info} reaches 45% at short integration times, set by the finite detection efficiency η . It falls to approximately 12% at the throughput-optimal integration point as accumulated T_1 relaxation events cause $C(\tau)$ to deviate from ideal Gaussian scaling.

B. Separation of Optimal Integration Times

Figure 3 shows the Bayes fidelity and total certification time as functions of τ for standard parameters. The fidelity peaks at $\tau_{\text{fid}} \approx 0.78 \mu\text{s}$, while the certification time for target error $\epsilon = 10^{-4}$ reaches its minimum at $\tau_{\text{rate}} \approx 1.22 \mu\text{s}$ — a substantially longer window.

The shift arises because T_{cert} accounts for both the information rate $C(\tau)$ and the fixed hardware overhead. Integrating longer reduces the total number of shots required to reach the certification threshold, more than compensating for the longer per-shot window. For the baseline parameters this yields a speedup of 1.11 \times over operating at the fidelity-optimal point.

C. Scaling and Global Performance Limits

Figure 4(a) maps the speedup factor across a range of T_1 times and detection efficiencies η . At fixed measurement efficiency, longer T_1 produces a modest increase in speedup, with the dependence on T_1 weaker than that on η or per-shot overhead. Longer coherence reduces decay-induced asymmetry, allowing more efficient information accumulation per shot.

The per-shot overhead τ_{oh} is the blocking idle time between successive integration windows, during which no new certification shot can begin — it includes qubit reset, passive thermalization, and classical control latency required to re-arm the measurement sequence. We take $\tau_{\text{oh}} = 15 \mu\text{s}$ as a representative mid-range value. Figure 5(b) sweeps τ_{oh} from 5–30 μs , covering optimized active-reset implementations at the low end [4, 48] and passive single- T_1 thermalization at the high end.

D. Consistency in the Gaussian Limit

Figure 5(a) validates the numerical framework in the limit $T_1 \rightarrow \infty$, where score distributions are symmetric Gaussians. The numerically computed Chernoff information C agrees with the analytical result $SNR^2/8$, confirming the internal consistency of the discretized integration procedure.

Even without qubit decay, τ_{fid} and τ_{rate} remain distinct [Fig. 5(b)]. In this limit the fidelity optimum shifts to $\tau_{\text{fid}} = 1.34 \mu\text{s}$, later than the $\tau_{\text{fid}} \approx 0.78 \mu\text{s}$ seen in Fig. 3, because the absence of T_1 smearing moves the Bayes-fidelity peak toward integration windows where the cavity has more fully rung up. The separation between τ_{fid} and τ_{rate} therefore reflects the difference between the single-shot Bayes-fidelity objective and the multi-shot Chernoff error-exponent objective, not an artifact of qubit relaxation. Increasing τ_{oh} amplifies the effect over the physically relevant range, with the speedup growing from 1.04 \times to 1.13 \times as τ_{oh} increases from 5 to 30 μs .

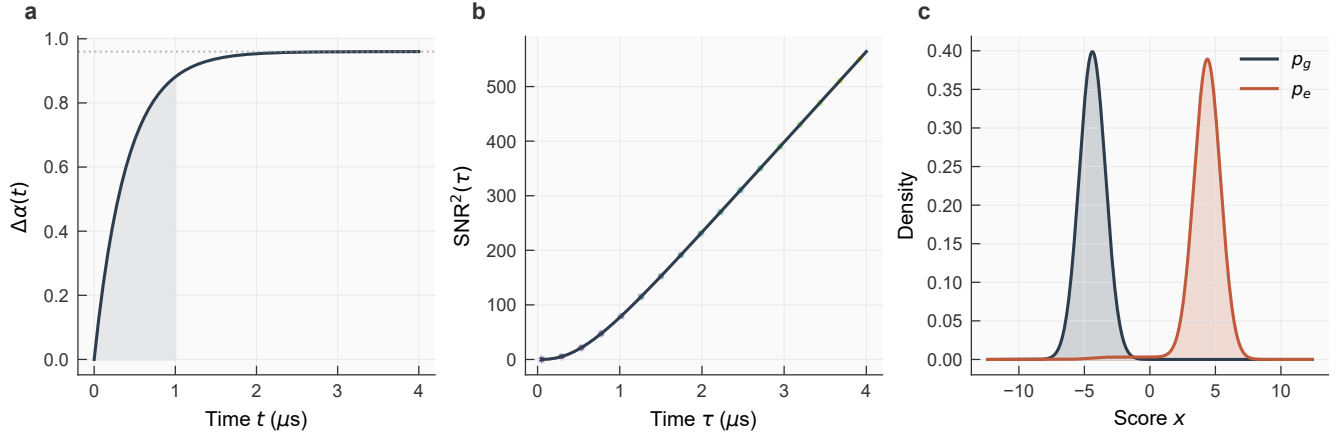


FIG. 1. **Dynamics of information accumulation in dispersive readout.** (a) Temporal evolution of the cavity coherent state separation $\Delta\alpha(t)$ following the onset of the drive pulse. The separation approaches the steady-state limit of $4\chi/\kappa$ as the resonator field rings up. (b) Integrated signal-to-noise ratio squared (SNR^2) as a function of integration time τ . The initial sublinear growth reflects the cavity ring-up phase, transitioning to a linear regime as the steady-state signal power is reached. (c) Score distributions $p_g(x)$ and $p_e(x)$ at $\tau = 1.0 \mu\text{s}$. While the ground-state distribution is nearly Gaussian, the excited-state distribution exhibits a tail extending toward the ground-state mean, a direct consequence of T_1 relaxation events occurring during the measurement window.

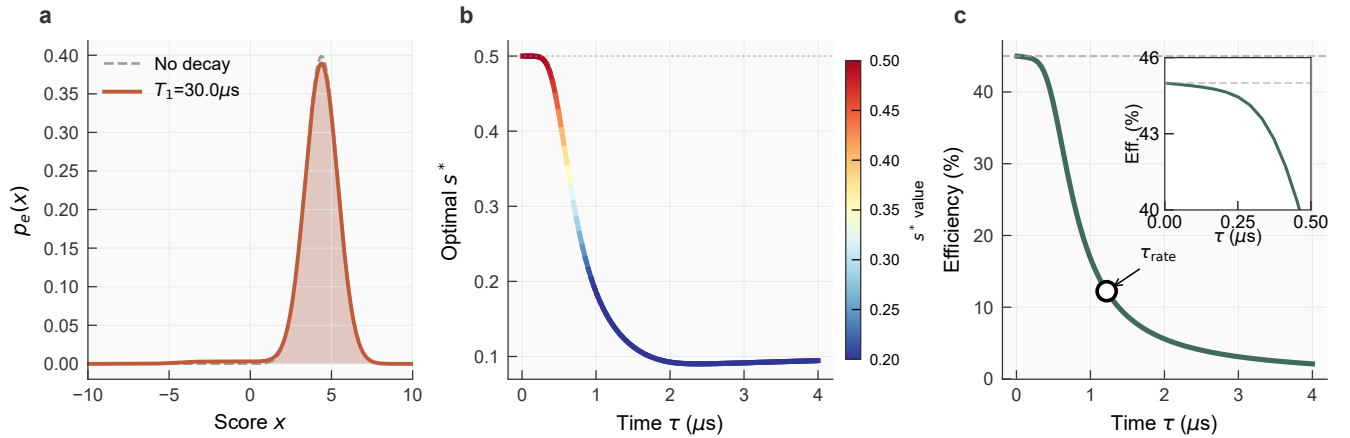


FIG. 2. **Characterizing T_1 -induced asymmetry and extraction efficiency.** (a) Comparison of the excited-state score distribution $p_e(x)$ in the ideal limit (no decay) and the realistic regime ($T_1 = 30 \mu\text{s}$). The relaxation events shift the score manifold, significantly displacing the optimal decision threshold. (b) The optimal Chernoff parameter s^* as a function of integration time. At short τ the distributions remain nearly symmetric ($s^* \approx 0.5$), but as decay events accumulate s^* shifts toward zero, indicating that the optimal classifier becomes more biased against the excited state. (c) Information extraction efficiency η_{info} relative to the unit-efficiency Gaussian Chernoff benchmark. The efficiency reaches its theoretical maximum of 45% at short integration times, limited by detection efficiency η , and falls monotonically as τ increases due to progressive T_1 -induced information loss.

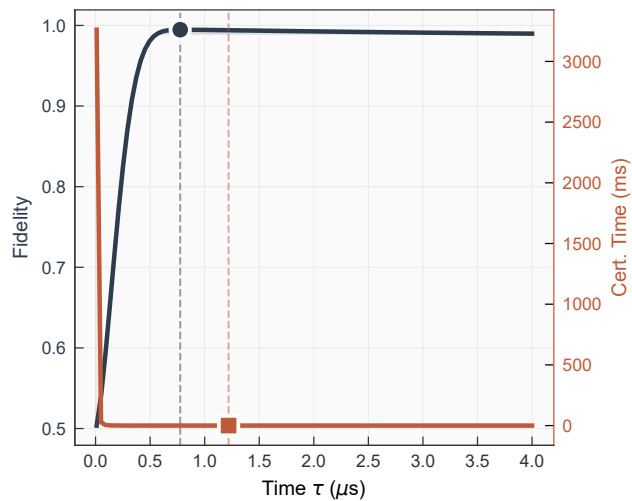


FIG. 3. **Separation between fidelity and certification-time optima.** Bayes fidelity (primary axis) and total wall-clock certification time (secondary axis) plotted against integration time τ for target error $\epsilon = 10^{-4}$. Vertical dashed lines indicate the fidelity-optimal point (τ_{fid}) and the certification-optimal point (τ_{rate}). The certification-time minimum occurs at a longer integration window, showing that throughput optimization trades single-shot confidence against per-shot hardware overhead.

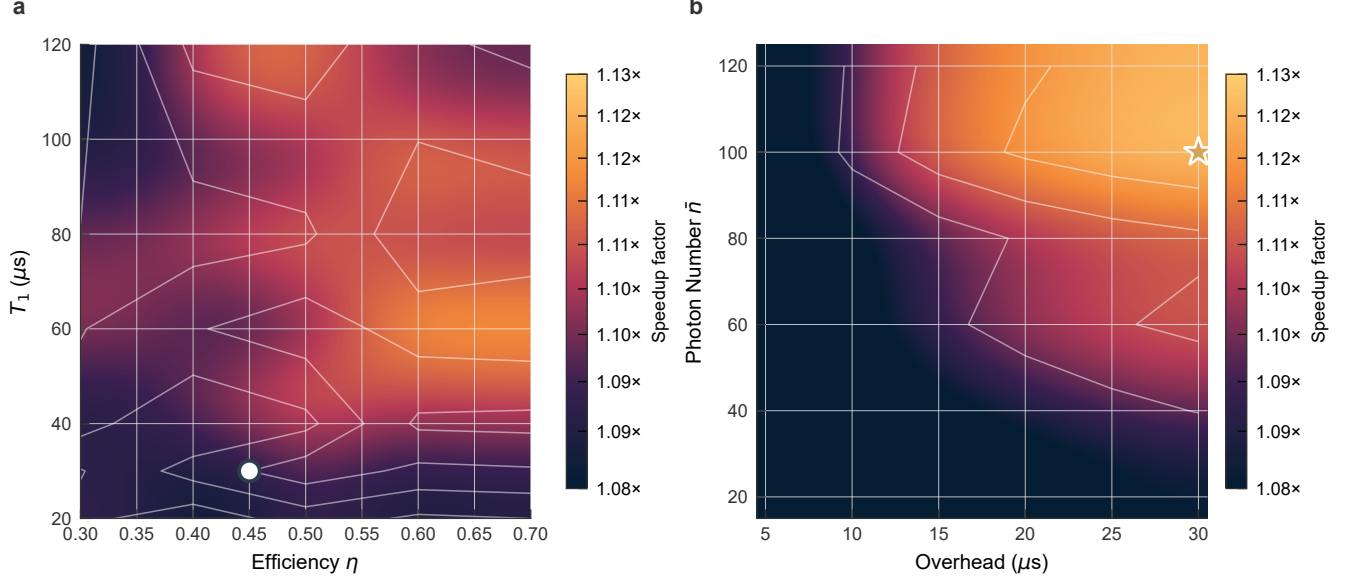


FIG. 4. **Scaling of certification speedup across parameter space.** (a) Speedup factor as a function of qubit relaxation time T_1 and detection efficiency η . Higher efficiencies allow the measurement to reach the certification threshold more rapidly, making the fixed hardware overhead the dominant bottleneck. The white circle marks the baseline parameters ($T_1 = 30 \mu\text{s}$, $\eta = 0.45$). (b) Speedup factor as a function of steady-state photon number \bar{n} and per-shot hardware overhead, evaluated at $T_1 = 20 \mu\text{s}$ and $\eta = 0.5$. The gold star marks the maximum speedup of 1.13x at $\bar{n} = 120$ and 30 μs overhead.

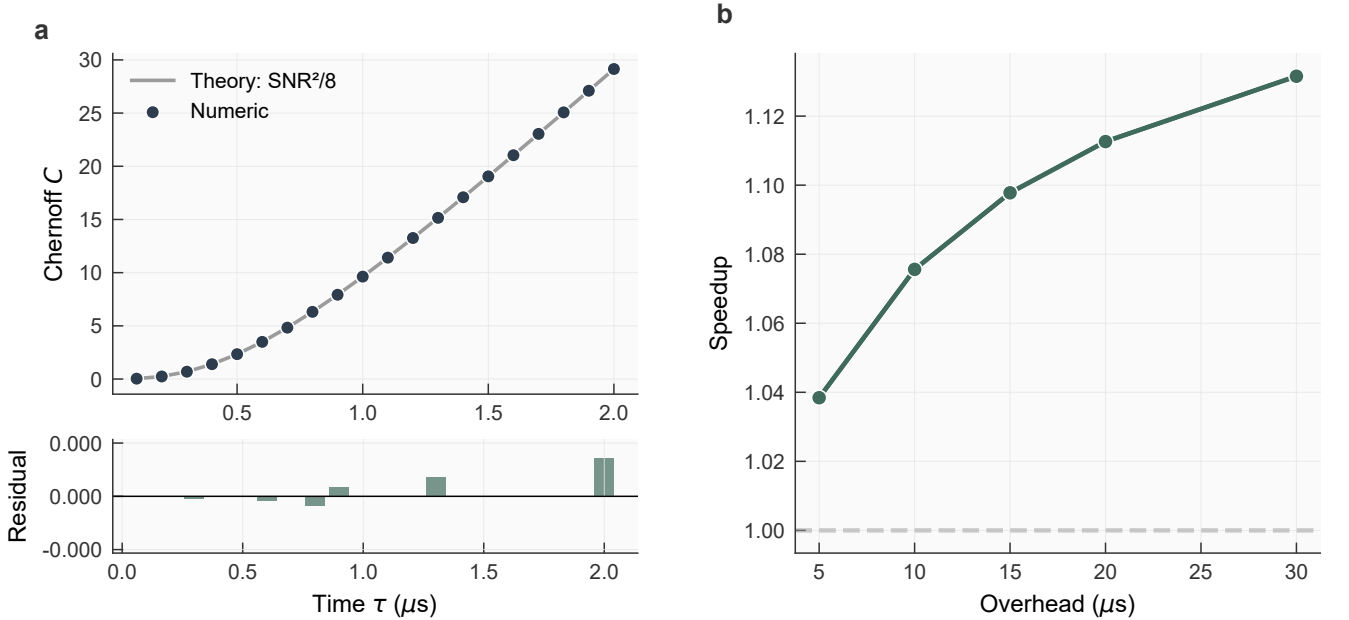


FIG. 5. **Framework validation and the Gaussian limit.** (a) Calculated Chernoff information C (points) compared to the analytical $\text{SNR}^2/8$ limit (line) with $T_1 \rightarrow \infty$. The lower panel shows residuals ($C_{\text{num}} - C_{\text{theory}}$), confirming numerical stability. (b) Speedup factor versus per-shot overhead in the $T_1 \rightarrow \infty$ limit. The overhead axis begins at 5 μs , since zero overhead is unphysical in realistic control stacks. The speedup increases monotonically with overhead, consistent with the amortization argument of Sec. II.D: τ_{rate} shifts to longer integration times while τ_{fid} is overhead-independent.

IV. CONCLUSION

Dispersive readout has traditionally been optimized by maximizing single-shot distinguishability. This is the wrong objective when the goal is to minimize total wall-clock certification time in a high-duty-cycle processor. Framing readout as a stochastic communication channel and optimizing the Chernoff error exponent directly reveals a consistent separation between the fidelity-optimal integration time τ_{fid} and the throughput-optimal time τ_{rate} .

This separation does not originate from qubit relaxation. The asymptotic analysis in the long-coherence Gaussian limit shows that any nonzero per-shot overhead τ_{oh} shifts the throughput optimum toward longer integration times. When fixed temporal costs are nonzero, extracting more information per shot reduces the total number of required repetitions enough to offset the longer window. Qubit relaxation during the measurement window introduces additional score asymmetry, modifying the Chernoff geometry and widening the gap between the two optima.

For representative transmon parameters, integrating

approximately 55% longer than the fidelity-optimal time reduces total certification runtime by roughly 9–11%. The achievable speedup is bounded, with a ceiling near $1.13\times$ across the parameter regimes studied, but it requires no hardware modification — only a recalibration of the integration window.

Benchmarking classical Chernoff extraction against the unit-efficiency Gaussian limit provides an experimentally accessible diagnostic for information loss. The sharp drop in extraction efficiency at the throughput-optimal point makes the distinct contributions of amplifier inefficiency and T_1 -induced trajectory smearing directly visible.

As superconducting processors scale and repetition rates increase, readout and reset latency will take up a growing share of total runtime. Calibrating the integration window against wall-clock certification time, rather than single-shot fidelity, directly addresses this bottleneck.

CODE AVAILABILITY

The numerical code used to generate the results in this study is available from the corresponding author upon reasonable request.

-
- [1] A. G. Fowler, M. Mariantoni, J. M. Martinis, and A. N. Cleland, Surface codes: Towards practical large-scale quantum computation, *Physical Review A* **86**, 032324 (2012).
 - [2] B. M. Terhal, Quantum error correction for quantum memories, *Reviews of Modern Physics* **87**, 307 (2015).
 - [3] R. Acharya and others (Google Quantum AI), Quantum error correction below the surface code threshold, *Nature* **638**, 920 (2025).
 - [4] S. Krinner, N. Lacroix, A. Remm, A. Di Paolo, E. Genois, C. Leroux, C. Hellings, S. Lazar, F. Swiadek, J. Herrmann, *et al.*, Realizing repeated quantum error correction in a distance-three surface code, *Nature* **605**, 669 (2022).
 - [5] F. Arute *et al.*, Quantum supremacy using a programmable superconducting processor, *Nature* **574**, 505 (2019).
 - [6] A. Blais, A. L. Grimsmo, S. M. Girvin, and A. Wallraff, Circuit quantum electrodynamics, *Reviews of Modern Physics* **93**, 025005 (2021).
 - [7] T. Walter, P. Kurpiers, S. Gasparinetti, P. Magnard, A. Potočnik, Y. Salathé, M. Pechal, M. Mondal, M. Oppliger, C. Eichler, and A. Wallraff, Rapid high-fidelity single-shot dispersive readout of superconducting qubits, *Physical Review Applied* **7**, 054020 (2017).
 - [8] F. Swiadek, R. Shillito, P. Magnard, *et al.*, Enhancing dispersive readout of superconducting qubits through dynamic control of the dispersive shift: Experiment and theory, *PRX Quantum* **5**, 040326 (2024).
 - [9] A. A. Clerk, M. H. Devoret, S. M. Girvin, F. Marquardt, and R. J. Schoelkopf, Introduction to quantum noise, measurement, and amplification, *Reviews of Modern Physics* **82**, 1155 (2010).
 - [10] J. Gambetta, A. Blais, M. Boissonneault, A. A. Houck, D. Schuster, and S. M. Girvin, Quantum trajectory approach to circuit qed: Quantum jumps and the zeno effect, *Phys. Rev. A* **77**, 012112 (2008).
 - [11] M. D. Reed, L. DiCarlo, B. Johnson, L. Sun, D. Schuster, L. Frunzio, and R. Schoelkopf, High-fidelity readout in circuit quantum electrodynamics using the jaynes-cummings nonlinearity, *Physical review letters* **105**, 173601 (2010).
 - [12] K. W. Murch, S. Weber, C. Macklin, and I. Siddiqi, Observing single quantum trajectories of a superconducting quantum bit, *Nature* **502**, 211 (2013).
 - [13] M. Hatridge, S. Shankar, M. Mirrahimi, F. Schackert, K. Geerlings, T. Brecht, K. Sliwa, B. Abdo, L. Frunzio, S. M. Girvin, *et al.*, Quantum back-action of an individual variable-strength measurement, *Science* **339**, 178 (2013).
 - [14] M. Féchant, M. F. Dumas, D. Bénâtre, N. Gosling, P. Lenhard, M. Spiecker, S. Geisert, S. Ihssen, W. Wernsdorfer, B. D’Anjou, *et al.*, Offset charge dependence of measurement-induced transitions in transmons, *Physical Review Letters* **135**, 180603 (2025).
 - [15] M. F. Dumas, B. Groleau-Paré, A. McDonald, M. H. Muñoz-Arias, C. Lledó, B. D’Anjou, and A. Blais, Measurement-induced transmon ionization, *Physical Review X* **14**, 041023 (2024).
 - [16] K. N. Nesterov and I. V. Pechenezhskiy, Measurement-induced state transitions in dispersive qubit-readout schemes, *Physical Review Applied* **22**, 064038 (2024).
 - [17] N. Didier, J. Bourassa, and A. Blais, Fast quantum non-demolition readout by parametric modulation of longitu-

- dinal qubit-oscillator interaction, *Physical review letters* **115**, 203601 (2015).
- [18] Y. Ye, J. B. Kline, S. Chen, A. Yen, and K. P. O'Brien, Ultrafast superconducting qubit readout with the qurton coupler, *Science Advances* **10**, eado9094 (2024).
- [19] A. Sah, S. Kundu, H. Suominen, Q. Chen, and M. Möttönen, Decay-protected superconducting qubit with fast control enabled by integrated on-chip filters, *Communications Physics* **7**, 227 (2024).
- [20] E. Jeffrey, D. Sank, J. Mutus, T. F. White, J. Kelly, R. Barends, Y. Chen, Z. Chen, B. Chiaro, A. Dunsworth, *et al.*, Fast accurate state measurement with superconducting qubits, *Physical review letters* **112**, 190504 (2014).
- [21] A. Bengtsson, A. Opremcak, M. Khezri, D. Sank, A. Bourassa, K. J. Satzinger, S. Hong, C. Erickson, B. J. Lester, K. C. Miao, A. N. Korotkov, J. Kelly, Z. Chen, and P. V. Klimov, Model-based optimization of superconducting qubit readout, *Physical Review Letters* **132**, 100603 (2024).
- [22] S. Hazra, W. Dai, T. Connolly, P. D. Kurilovich, Z. Wang, L. Frunzio, and M. H. Devoret, Benchmarking the readout of a superconducting qubit for repeated measurements, *Physical Review Letters* **134**, 100601 (2025).
- [23] J. Heinsoo, S. Krinner, C. K. Andersen, A. Remm, S. Lazar, S. Krinner, and A. Wallraff, Rapid high-fidelity multiplexed readout of superconducting qubits, *Physical Review Applied* **10**, 034040 (2018).
- [24] P. A. Spring, L. Milanovic, Y. Sunada, S. Wang, A. F. van Loo, S. Tamate, and Y. Nakamura, Fast multiplexed superconducting-qubit readout with intrinsic purcell filtering using a multiconductor transmission line, *PRX Quantum* **6**, 020345 (2025).
- [25] C. C. Bultink, M. A. Rol, T. E. O'Brien, X. Fu, S. de Jong, C. Dickel, A. Bruno, N. K. Langford, and L. DiCarlo, Active resonator reset in the nonlinear dispersive regime of circuit qed, *Physical Review Applied* **6**, 034008 (2016).
- [26] M. A. Castellanos-Beltran, K. D. Irwin, G. C. Hilton, L. R. Vale, and K. W. Lehnert, Amplification and squeezing of quantum noise with a tunable josephson metamaterial, *Nature Physics* **4**, 929 (2008).
- [27] C. Macklin, K. O'Brien, D. Hover, M. Schwartz, V. Bolkhovskiy, X. Zhang, W. D. Oliver, and I. Siddiqi, A near-quantum-limited josephson traveling-wave parametric amplifier, *Science* **350**, 307 (2015).
- [28] S. Bugu, Resilience of entanglement-induced coordination in adversarial environments: The team-based quantum sabotage game, *arXiv preprint arXiv:2510.22444* (2025).
- [29] S. Bugu, Hidden-field coordination reveals payoff-free quantum correlation structure in decentralized coordination (2026), *arXiv:2601.21139 [quant-ph]*.
- [30] D. Ristè, C. Bultink, K. W. Lehnert, and L. DiCarlo, Feedback control of a solid-state qubit using high-fidelity projective measurement, *Physical review letters* **109**, 240502 (2012).
- [31] K. T. Goh, J. Kaniewski, E. Wolfe, T. Vértési, X. Wu, Y. Cai, Y.-C. Liang, and V. Scarani, Geometry of the set of quantum correlations, *Physical Review A* **97**, 022104 (2018).
- [32] B. D'Anjou, Generalized figure of merit for qubit readout, *Physical Review A* **103**, 042404 (2021).
- [33] H. Chernoff, A measure of asymptotic efficiency for tests of a hypothesis based on the sum of observations, *The Annals of Mathematical Statistics* **23**, 493 (1952).
- [34] M. Nussbaum and A. Szkola, The chernoff lower bound for symmetric quantum hypothesis testing, *Annals of Statistics* **37**, 1040 (2009).
- [35] S. Boutin, C. K. Andersen, J. Venkatraman, A. J. Ferris, and A. Blais, Resonator reset in circuit qed by optimal control for large open quantum systems, *Physical Review A* **96**, 042315 (2017).
- [36] K. M. Audenaert, J. Calsamiglia, R. Muñoz-Tapia, E. Bagan, L. Masanes, A. Acín, and F. Verstraete, Discriminating states: The quantum chernoff bound, *Physical review letters* **98**, 160501 (2007).
- [37] S. Pirandola and S. Lloyd, Computable bounds for the discrimination of gaussian states, *Physical Review A—Atomic, Molecular, and Optical Physics* **78**, 012331 (2008).
- [38] D. Sank, Z. Chen, M. Khezri, J. Kelly, R. Barends, B. Campbell, Y. Chen, B. Chiaro, A. Dunsworth, A. Fowler, *et al.*, Measurement-induced state transitions in a superconducting qubit: Beyond the rotating wave approximation, *Physical review letters* **117**, 190503 (2016).
- [39] Y. Sunada, Y. Kono, S. Wang, Z. Ilves, T. Miyamura, J. Matsuura, S. Tamate, and Y. Nakamura, Photon-noise-tolerant dispersive readout of a superconducting qubit using a nonlinear purcell filter, *PRX Quantum* **5**, 010307 (2024).
- [40] A. Blais, S. M. Girvin, and W. D. Oliver, Quantum information processing and quantum optics with circuit quantum electrodynamics, *Nature Physics* **16**, 247 (2020).
- [41] J. Preskill, Quantum computing in the nisq era and beyond, *Quantum* **2**, 79 (2018).
- [42] A. W. Harrow and A. Montanaro, Quantum computational supremacy, *Nature* **549**, 203 (2017).
- [43] A. Opremcak, C. Liu, C. Wilen, K. Okubo, B. Christensen, D. Sank, T. White, A. Vainsencher, M. Giustina, A. Megrant, *et al.*, High-fidelity measurement of a superconducting qubit using an on-chip microwave photon counter, *Physical Review X* **11**, 011027 (2021).
- [44] T. M. Cover and J. A. Thomas, *Elements of Information Theory* (Wiley-Interscience, 2006).
- [45] E. Rosenthal, C. Schneider, M. Malnou, Z. Zhao, F. Leditzky, B. Chapman, W. Wustmann, X. Ma, D. Palken, M. Zanner, *et al.*, Efficient and low-backaction quantum measurement using a chip-scale detector, *Physical Review Letters* **126**, 090503 (2021).
- [46] R. Barends, J. Kelly, A. Megrant, D. Sank, E. Jeffrey, Y. Chen, Y. Yin, B. Chiaro, J. Mutus, C. Neill, *et al.*, Coherent josephson qubit suitable for scalable quantum integrated circuits, *Physical review letters* **111**, 080502 (2013).
- [47] C. C. Bultink, M. Rol, T. O'Brien, X. Fu, B. Dikken, C. Dickel, R. Vermeulen, J. De Sterke, A. Bruno, R. Schouten, *et al.*, Active resonator reset in the nonlinear dispersive regime of circuit qed, *Physical Review Applied* **6**, 034008 (2016).
- [48] P. Magnard, P. Kurpiers, B. Royer, T. Walter, J.-C. Besse, S. Gasparinetti, M. Pechal, J. Heinsoo, S. Storz, A. Blais, and A. Wallraff, Fast and unconditional all-microwave reset of a superconducting qubit, *Phys. Rev. Lett.* **121**, 060502 (2018).